Int. J. Heat Mass Transfer. Vol. 36, No. 15, pp. 3751–3758, 1993
Printed in Great Britain

0017–9310/93 $6.00+0.00

Measurements of flow structure in the radial layer of impinging free-surface liquid jets

J. STEVENS† and B. W. WEBB
Heat Transfer Laboratory, Department of Mechanical Engineering,
Brigham Young University, Provo, UT 84602, U.S.A.

(*Received* 16 *June* 1992 *and in final form* 5 *March* 1993)

Abstract—The thin radial-flow layer formed by a free-surface liquid jet impinging normally against a flat surface was studied experimentally using laser-Doppler velocimetry to make velocity and turbulence measurements across the layer depth. Significant insights into the nature of the radial-flow region of an impinging jet are reported. For radial locations of less than 2.5 nozzle diameters, the velocity profiles showed that the maximum velocity in the layer occurred very near the plate, contrary to the assumption common to analytical treatments that the velocity outside the boundary layer is everywhere equal to the pre-impingement jet velocity. Analytical predictions of the layer velocity profile, the layer depth, and the free-surface velocity, were compared to experimental measurements. Turbulence measurements from within the layer were reported. Turbulence was found to increase near the plate, and an apparent transition to turbulent flow was documented.

INTRODUCTION

IMPINGING jets are characterized by unusually high transfer coefficients near the stagnation region. For this reason, they have found wide application in a variety of industries. They are used in the glass and metal industries for cooling, and in the paper and textile industries for drying, and for thermal control of high heat flux electronic equipment. Inasmuch as the heat and mass transfer beneath an impinging jet depend on the nature of the flow field, a full understanding of the flow is a prerequisite to understanding the associated transport phenomena. While the flow structure for submerged jets, in general, and for air jets in particular, has been studied extensively in the literature for the cases of both impinging and non-impinging jets, free liquid jets have received comparatively little attention. Any analytical treatment of the heat transfer under an impinging liquid jet relies upon assumptions about the flow. For the radial flow region of an impinging jet, many of these assumptions remain unsubstantiated by experimental evidence. The objective of this research is to experimentally characterize the radial flow region of an axisymmetric free liquid jet impinging normally against a flat surface by measuring local velocity and turbulence levels in the layer.

Watson appears to have been the first to examine analytically the laminar and turbulent radial spread of a liquid jet over a flat impingement surface out to, and including, the hydraulic jump using boundary layer theory [1]. A similarity solution was developed of the form $u = U(r)f(\eta)$ where $\eta = z/h(r)$, $h(r)$ is the local layer thickness, and $f(\eta)$ is the similarity function. The flow was considered in four regions as follows:

1. A region of radial extent of order $d/2$ where the speed outside the boundary layer rises rapidly from 0 at the stagnation point to U_0 ($= V_j$ in the absence of gravitational effects), the pre-impingement jet velocity.
2. A region where the flow assumes the Blasius flat plate profile inside the boundary layer and remains at U_0 outside the boundary layer.
3. A transition region where the boundary layer reaches the free surface and the velocity profile changes from the Blasius flat plate profile to Watson's similarity solution profile.
4. A region where the boundary layer has absorbed the whole flow and Watson's similarity profile is valid.

It was shown that, to a good approximation (within 6%), the transition region (region 3) could be handled by using Watson's similarity profile with $U(r) = U_0$ and $\eta = z/\delta$. Turbulent flow was also considered using an eddy viscosity model and proceeding analogously to the development for laminar flow. The flow of a planar liquid jet was discussed as well.

Nakoryakov *et al.* discussed the radial layer flow field of an impinging liquid jet in an experimental and theoretical study on the mass transfer and friction factor under such a jet [2]. The four regions described by Watson [1] were used in the theoretical development.

Thomas *et al.* experimentally studied the radial flow originating from a pressurized container on a rotating and stationary disk [3]. For the stationary configuration, before the hydraulic jump, it was found that the film thickness either increased monotonically

† Currently at Department of Mechanical Engineering, Mississippi State University.

NOMENCLATURE

d	nozzle diameter
h	local radial-flow layer thickness
M	constant from integration of radial velocities across the layer depth, equation (3)
Q	volume flow rate
r	radial coordinate measured from the stagnation point
r_0	radial location where the boundary layer reaches the free surface
Re	Reynolds number, $4Q/\pi\nu d$
u	local mean velocity in the radial direction
$\bar{u}$	spatial average radial velocity across liquid layer depth, $\frac{1}{h}\int_0^h u(z)\,dz$
U	local mean surface velocity on the radially spreading liquid layer
u'	local RMS fluctuation in the radial direction
U'	local RMS fluctuation in U
V_j	average jet exit velocity, $4Q/\pi d^2$
x	constant of integration from the analysis of Carper [9]
z	axial coordinate measured from the impingement plate.

Greek symbols

δ	local momentum boundary layer thickness
η	dimensionless axial coordinate measured from the plate
ν	fluid kinematic viscosity.

(lower flow rates), or decreased slightly, then increased (higher flow rates). A radial flow layer with and without rotation and gravity was also investigated numerically [4]. A uniform velocity profile was used as the inlet condition. Numerical calculations were carried out for this case by Rahman *et al.* [5] using boundary conditions determined by the measurements of Thomas *et al.* [3]. Predictions showed that, well upstream from the hydraulic jump, the liquid layer was characterized by a parabolic velocity profile. Rahman *et al.* performed a numerical study of a thin layer of fluid issuing radially from a pressurized cylinder, which included the hydraulic jump region [6]. It was found that the liquid layer thickness decreased monotonically from the discharge out to the hydraulic jump. Rahman *et al.* calculated a numerical solution for the heat transfer in the radial flow layer [7].

Liu and Lienhard used an integral method to analytically predict the heat transfer in a radial layer flow [8]. Experiments were performed to validate the analytical models. A cubic velocity profile across the liquid layer depth was employed.

Carper examined two approximate solutions to the laminar momentum equations for a free liquid impinging jet as part of a larger study of the heat transfer in such a configuration [9]. One of the approximate solutions was that of Watson, discussed above. The author improved on a previous solution from Hung [10] by using a better initial condition, and found that it agreed well with the results of Watson.

Olsson and Turkdogan examined experimentally the radial flow field of an impinging liquid jet [11]. Dimensionless nozzle-to-plate spacings (z/d) of 26 and 64 were used, and experiments included a variety of liquids with varying viscosities. A Vernier height gauge was used to measure the local liquid layer depth. Surface velocities were measured by using tracer particles and high speed photography. Measurements were conducted on the flow both prior to, and after, the hydraulic jump. It was concluded that the boundary layer had not yet reached the free surface at the hydraulic jump for the configurations examined. This implied that it must reach the free surface much later than indicated by the predictions of Watson. In addition, it was found that the surface velocity of the liquid layer was constant out to the hydraulic jump, and significantly less than the mean velocity of the falling stream.

Azuma and Hoshino reported LDV measurements inside the radial liquid layer formed by placing an axisymmetric nozzle close to a flat plate (results were reported for dimensionless nozzle-to-plate spacings of 0.07, 0.08 and 0.3) [12]. It was found that the radial film flow begins with a laminar boundary layer, which eventually reaches the free surface, absorbing the entire flow. For sufficiently large Re, the laminar flow later changes to a turbulent flow so that the entire flow is a turbulent boundary layer. A fourth-order polynomial assumption for the velocity profile fits the measured velocities best in the region of the laminar boundary layer, while Watson's profile fits the flow better in the region where the laminar boundary layer engulfed the entire flow.

Stevens and Webb measured free-surface velocity distributions, $U(r)$, from an impinging liquid jet with laser-Doppler velocimetry [13]. It was found that the free-surface velocities of the radial layer flow would collapse to a single band independent of nozzle size and flow rate when plotted in dimensionless coordinates: U/V_j vs r/d. This band was correlated to $\pm 20\%$ by a parabola matched with a straight line:

$$0.5 \leqslant r/d \leqslant 2.86$$

$$U/V_j = -0.125(r/d)^2 + 0.625(r/d) + 0.303 \quad \text{(1a)}$$

$$2.86 \leqslant r/d \leqslant 14$$
$$U/V_j = -0.0936(r/d) + 1.33. \quad (1b)$$

The band of correlated velocities contained a maximum at $r/d \approx 2.5$. It was demonstrated that the layer depth could be expressed as

$$\frac{h}{d} = \left(\frac{1}{8M}\right)\left(\frac{1}{r/d}\right)\left(\frac{1}{U/V_j}\right) \quad (2)$$

where

$$M = \int_0^1 f(\eta)\,d\eta = \bar{u}/U. \quad (3)$$

In equation (3), $\eta = z/h$ and $f(\eta) = u/U$ is an assumed velocity profile across the layer. Several profiles were discussed, with a corresponding unique value of the constant M in equation (3).

Recently, flow structure and local heat transfer measurements were reported in the stagnation zone of free-surface liquid jets with different nozzle types [14, 15]. The study revealed experimentally the coupling between the hydrodynamic flow structure and the corresponding transport in the region $0 \leqslant r/d \leqslant 0.5$.

It is clear from the preceding discussion that direct experimental measurements of the flow structure would provide valuable assumption validation and insight into the nature of the radial layer flow of an impinging free-surface liquid jet. Such information is critical to the understanding of the transport, since the heat and momentum transport are so intimately coupled. This is particularly true of turbulent flow, which is so difficult to characterize analytically. The objective of this study was to experimentally explore this region of the jet flow field by measuring velocity and turbulence profiles across the depth of the radially spreading liquid layer.

METHOD AND EXPERIMENTAL APPARATUS

The impinging jet was formed in a closed loop system containing a pump, flow meters, a nozzle, and apparatus for collecting spent water and directing it back to the pump. The pump had a maximum capacity of 53 lpm at 0.069 MPa and 7.6 lpm at 1.1 MPa. A bypass circuit was included in order to allow the pump to operate at optimal conditions while maintaining the jet at the desired flow rate. The flowmeters were King Instrument Co. K72 series rotameters with a combined measurement range of 0.38–45.6 lpm (0.1–12 gpm) with an uncertainty of 0.038 lpm for flow rates less than 3.8 lpm and an uncertainty of 0.38 lpm for flow rates greater than 3.8 lpm. The average jet exit velocity was calculated from the flow meter readings and the known nozzle diameter. The flow loop is described in greater detail elsewhere [16].

Liquid velocities were measured with a TSI laser-Doppler velocimeter using a Spectra-Physics 5 Watt Argon-Ion laser. The optics were configured for back-scatter operation, as illustrated in Fig. 1. Only one component of the velocity was measured in this study, using the 488 nm (blue) line of the laser. The optical train included a field stop system with an aperture of 0.20 mm. A 120 mm focal distance lens was used with beam expansion to provide a measurement volume with a calculated size of approximately 0.16 mm × 0.03 mm. Coarse measurements indicated that, for the power settings and flow situations of this study, the actual length of the major axis was approximately 0.3 mm for this configuration. Photodetector output was processed by a TSI model 1980B signal processor operating in continuous data collection mode. Frequency shifting at one MHz was employed to improve the data rate and minimize fringe bias. A microcomputer was used to process and store the data. Typically, three to five thousand instantaneous velocity points were used in determining the local mean and RMS velocity. The measurement volume was moved relative to the stationary experimental setup by moving the entire LDV system on a three-axis traversing table with ±0.1 mm resolution in each direction.

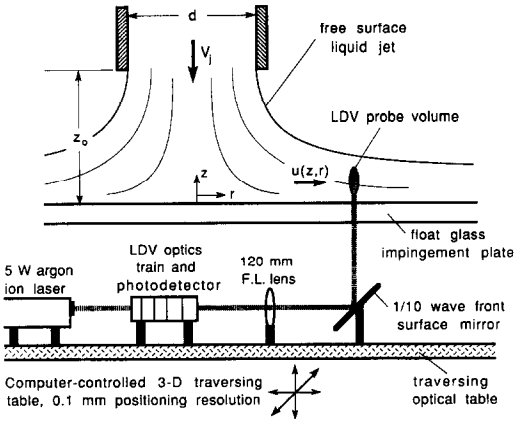

FIG. 1. Schematic diagram of experimental apparatus.

A tenth-wave, front surface mirror was used to reflect the laser beams from below through a glass impingement plate so that the measurement volume was positioned inside the liquid jet. The flow was seeded with milk at a very low concentration. The concentration was deliberately low so that measurements could be taken well above the impingement plane without interference from excessive light scattering through the fluid. The radial coordinate was established for each measurement configuration (Re and d) by initially positioning the measurement volume to one side of the jet centerline, then taking closely spaced velocity measurements as the LDV diagnostic volume was traversed radially across the centerline. The stagnation streamline ($r = 0$) was then determined by interpolating to locate the point where the measured velocity was exactly zero. Velocity profiles were measured across the liquid layer at each radial location by initially positioning the measurement volume as close to the plate as possible, then

Table 1. Measurement configurations

Nozzle diameter (mm)	23.0	14.0	10.9	14.0	7.6
Reynolds number	37000	25800	33200	2600	13300
	25900	36100	40000	5200	17100
	11000	46400	46500	10300	22800
			53100		

making measurements in a line normal to the impingement plane.

The nozzles consisted of pipes of sufficient length so that the turbulent pipe flow was fully developed at the nozzle exit. The nozzle-to-plate spacing was maintained at one nozzle diameter for all cases except the 23.0 mm nozzle, for which it was three-quarters of a nozzle diameter. Maximum uncertainty in the average jet velocity (measured with the flowmeters) is estimated to be 7%. Uncertainty in the local velocity measurements (measured with the LDV) is estimated to be less than 4%.

The nozzle and flow rate configurations at which measurements were made are shown in Table 1. Nozzle diameters used in the study ranged between 7.6–23.0 mm i.d., and flow rates were between 0.5–25 lpm. These nozzle sizes and flow rates were used in combinations to provide an approximate Reynolds number range of 2600–53 100.

RESULTS AND DISCUSSION

Measurement procedure

There were numerous problems associated with taking data in the radial layer flow at $r/d > 0.5$. The layer was very thin, so even though the measurement volume length was estimated to be only 0.3 mm, in some instances only one or two independent (non-overlapping) measurements could be made through the thickness of the liquid layer. Furthermore, it was virtually impossible to determine when the measurement volume had penetrated the free-surface as the table was traversed vertically. This was because the air–water interface reflected the measurement volume back into the liquid layer as the interface was reached. Finally, a large zero-velocity spike was observed in the velocity histogram as the air–water interface was approached. This was also due to the backward scattering of the laser beams from the interface which effectively positioned the reflected measurement volume at the stationary wall. The problem of locating the free surface was also encountered by Azuma and Hoshino [12], and is described in great detail in their paper. In that reference, however, the layer was much thicker and the interface was apparently smoother so that a change in the data rate could be used to ascertain when the measurement volume had reached the free surface. For this study, other methods were employed. In order to remove the zero-velocity spike from the collected data, a histogram was plotted for each velocity measurement as demonstrated by Fig. 2. The extent of the zero velocity spike was determined, and those data with Doppler frequency equal to the shift frequency selected (indicating erroneous zero velocity caused by reflection of the LDV diagnostic volume off the liquid free surface and onto the stationary impingement plate) were removed digitally in the data file. The mean and RMS velocities were then recalculated from the reduced set. As shown by the example in Fig. 2, there was a clear break between the fluid velocities and the unwanted zero-velocity signal corresponding to unwanted wall measurements. This break was present in all measurements used, including those close to the impingement plate, which implies that all measured velocities were sufficiently far from the wall that near-zero flow velocities from the boundary layer were not included. In principle, it should have been possible to adjust the filter bank on the signal processor to eliminate the unwanted signal as the data was collected. However, in practice, the fixed and discrete filter settings on the signal processor made it more convenient to filter the data digitally in software as described. The problem of determining the depth of the air–water interface was handled by traversing vertically until no further signal was received. Then, the average depth of the layer was determined by integrating the measured velocities in the z-direction until integral continuity for the axisymmetric configuration was satisfied for the given r-location, r_i:

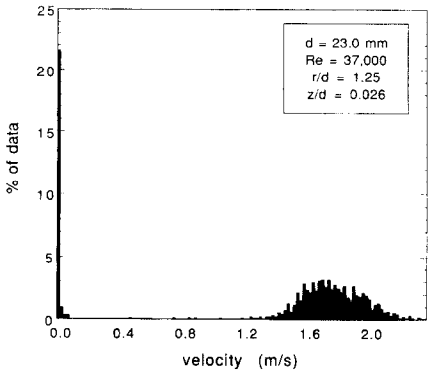

FIG. 2. Sample velocity histogram from the radial flow measurements, $Re = 37000$, $d = 23.0$ mm, $r/d = 1.25$, $z/d = 0.026$.

$$\frac{V_j \pi d^2}{4} = 2\pi r_i \int_0^h u(z)\,dz. \tag{4}$$

Axisymmetry was verified by rotating the nozzle with respect to the measurement volume, and repeating the measurement. Measurements were attempted in the liquid layer radially beyond the hydraulic jump as well. However, the difficulties described above were compounded by the very slow fluid velocities of that region. These velocities resulted in an unacceptably low data rate and also made it impractical to cleanly

filter the desired signal from the zero-velocity spike at the wall.

In spite of the difficulties described above in collecting data through the spreading liquid layer, the available measurements yield valuable results for characterizing the flow field through this region.

Mean velocity

Figure 3 exhibits samples of the data in the radial-flow layer for nozzles of $d = 10.9$ and 23.0 mm. The largest nozzle provided the thickest layer (see equations (1) and (2)), and thus gave the greatest measurement resolution, and consequently, the most complete and detailed results. These figures show all of the data taken, some of which, as discussed previously, correspond to measurement volume locations above the free surface of the liquid layer. The average free surface location determined according to equation (4) is also shown in the figures. Note that the radial spacing between the vertical scans is not plotted to scale in these figures. The data from the 23.0 mm diameter nozzle provides a much clearer picture of the flow profile through the liquid layer, but is limited to a relatively small radial range ($0.5 \leqslant r/d \leqslant 2.25$). The data from the smaller nozzle cover a larger r/d range, but in some cases have only one or two points from within the layer. The profiles do serve to clarify some of the features of the radially spreading liquid layer from Stevens and Webb [13]. For example, the maximum in the plot of the dimensionless surface velocity as a function of r/d can be readily explained by examining the profiles of Fig. 3. It is clear that for small r/d the maximum velocity in the layer is close to the plate. Thus, the surface velocity is relatively low.

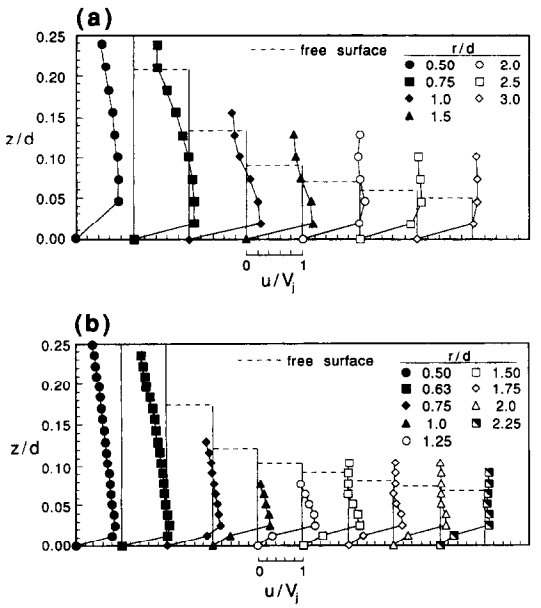

FIG. 3. Profiles of local radial velocity across the liquid layer depth for $Re = 37000$: (a) $d = 10.9$ mm, and (b) $d = 23.0$ mm.

As the fluid travels radially, the maximum velocity moves upward while the layer thins until the two meet and the maximum velocity is at the free surface near $r/d \approx 2.5$. This agrees with the maximum in the free-surface velocity data represented by equation (1). Careful examination of Fig. 3 shows that as the maximum velocity moves toward the free surface, the magnitude of this maximum decreases with radial distance for $r/d > 2$. This agrees qualitatively with the shape of the free-surface velocity profile of Stevens and Webb [13], and confirms that the monotonic decrease in the data of that study for $r/d > 2.5$ is a result of the retarding influence of the wall. In effect, the boundary layer absorbs the whole flow near $r/d \approx 2.5$. Note that the boundary layer discussed here is growing in an inertia-driven, zero-pressure gradient radial flow, and thus may differ from the more common boundary layers resulting from pressure-driven, two-dimensional flows. The invalidation of the common assumption of $u = V_j$ everywhere outside the boundary layer (for example, Watson [1]) reported by Stevens and Webb [13] is emphasized again by Fig. 3. For $r/d < 2.5$, not only is the maximum velocity not at the free surface of the flow, it is actually very close to the plate in this region. Note also that the maximum radial velocity in the layer has a magnitude greater than the average jet exit velocity, in some cases being 30% higher than V_j. This is consistent with previous measurements of the free-surface velocity, which were also observed to be greater than V_j.

These measurements also shed some light on possible velocity profile assumptions used in Stevens and Webb [13]. At small r/d the maximum velocity is near the plate, and the measured velocity profiles are very dissimilar to any of the analytic profile assumptions discussed. Thus, the expressions given for the velocity distribution across the liquid layer depth given [13] are clearly inappropriate descriptions for the velocity profiles across the radially spreading layer for $0.5 < r/d < 2.5$. At larger r/d, the liquid layer was generally too thin to obtain enough spatially resolved measurements to make a proper comparison between the equations and the data. However, near $r/d \approx 2.0$ for the 23.0 mm nozzle, there are sufficient data to make a rough comparison possible. Figure 4 com-

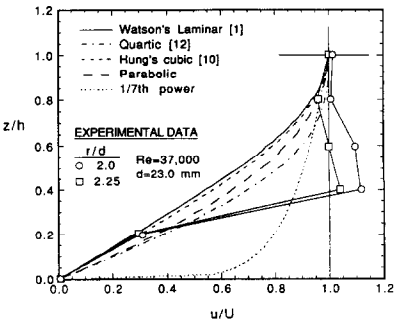

FIG. 4. Comparison of possible analytical velocity profiles across the liquid layer with experimental data.

pares two sets of measured velocities with various profiles from reported free-surface velocity measurements [13]. In Fig. 4, both the profiles and the data are plotted in dimensionless coordinates of u/U and z/h, where U is the free-surface velocity, and h is the local depth of the liquid layer. While the data are sparse, it appears that the difference between different profiles is small compared with the difference between the profiles and the data. It must be noted, however, that the measured velocities correspond to the region $r/d < 2.5$, and the maximum velocity has still not reached the free surface. Due to limitations of the experimental apparatus, it was not possible to make measurements at larger r/d for the largest nozzle. Further, for smaller nozzles the liquid layer was too thin to obtain velocity data providing a complete description of the velocity profile across its depth.

Layer depth and surface velocities

Figure 5 shows the local liquid layer depths, $h(r)/d$, calculated by integrating the measured radial velocity profiles according to equation (4). Also shown is the depth predicted using the correlation equation from the free-surface measurements of Stevens and Webb [13]. Finally, layer depths predicted previously [1, 9, 10] are included. The solution of Carper [9] contained a constant of integration, x, which was estimated by two different methods, resulting in possible values of 0.5 and 0.8. The lower panel of Fig. 5 shows one set of measurements from the 23.0 mm nozzle and one set from the 14.0 mm nozzle. The analytical expressions from Carper, Watson, and Hung are evaluated for $Re = 36\,500$. Watson's laminar solution, and the expression from Carper with the $x = 0.5$ provide the best overall agreement with the integrated data. The expression from the free-surface correlation is very poor at small r/d, but somewhat better, though still high, at larger r/d. This could be expected from the obvious shape difference between the assumed parabolic velocity profile of Stevens and Webb [13], and the velocity profiles at small r/d in Fig. 3. Also note that the free-surface data are represented by a correlation, which predicted the measured data only to within $\pm 20\%$. The upper panel of Fig. 5 shows a similar

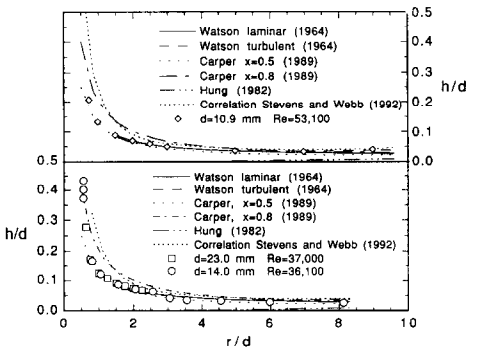

FIG. 5. Comparison of analytical predictions for the liquid layer depth with measurements.

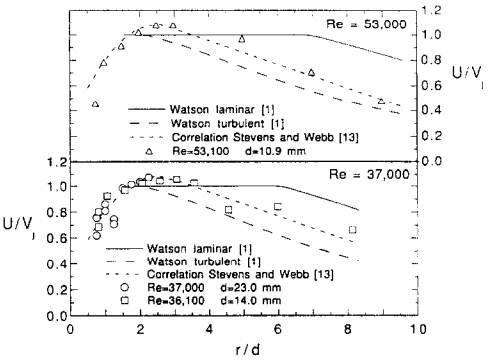

FIG. 6. Comparison of analytical predictions for the free-surface velocity with measurements.

comparison for a different nozzle and Reynolds number. For this case, the Watson laminar and turbulent expressions predict the depths best for smaller r/d, and the Watson turbulent expression and the expression from the free-surface measurements give the best prediction at larger r/d. The free-surface correlation and the Watson turbulent expression both accurately reflect the experimentally determined increase in depth at larger r/d.

Figure 6 compares the correlation from the measured free-surface velocities of ref. [13], equation (1), with linearly extrapolated free-surface velocities from the measurements of this study for the same configurations used in Fig. 5. The analytical expressions of Watson [1] for the free-surface velocity are also included for comparison. The interpolated velocities clearly validate the correlation equations of the previous work, particularly considering the width of the band of data that the correlation equations represent. Note that the dimensionless interpolated velocities at the free surface from this study are greater than unity as observed for the measured free-surface velocities [13]. These results confirm the validity of the more extensive measurements of the free-surface velocity of that study.

Turbulence

Figure 7 demonstrates the turbulence across the liquid layer for a subset of the same data as shown in Fig. 3. The figure shows the RMS turbulence (the RMS fluctuations normalized by the average jet exit

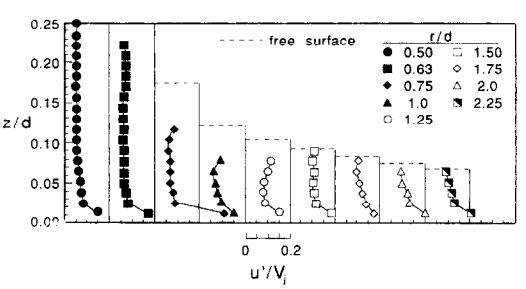

FIG. 7. Profiles of normalized RMS turbulence (u'/V_j) across the liquid layer depth for $Re = 37\,000$, $d = 23.0$ mm.

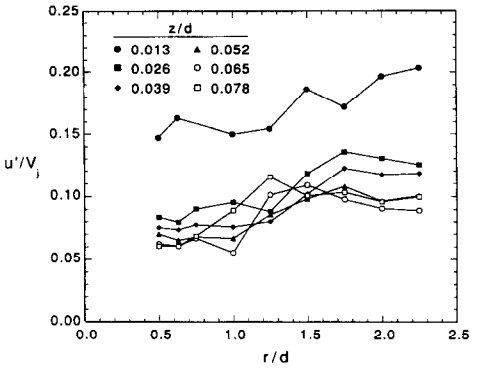

FIG. 8. Variation of the RMS turbulence (u'/V_j) vs radial location for $Re = 37\,000$, $d = 23.0$ mm.

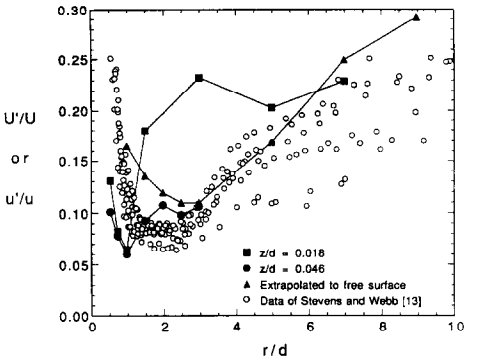

FIG. 10. Variation in turbulence intensity (u'/u) with radial position for $Re = 53\,100$, $d = 10.9$ mm, and comparison with previous free-surface measurements [13].

velocity) as a function of z/d and radial location for the 23.0 mm nozzle at $Re = 37\,000$. Only measurements from within the liquid layer are included in Fig. 7 and the local mean layer depths are duplicated from Fig. 3. Generally, the turbulence increases both near the wall and as one proceeds radially away from the stagnation point. This is shown more clearly in Fig. 8, where measurements from Fig. 7 are plotted as a function of r/d at distinct z/d.

In order to effectively display the turbulence levels in greater detail, the radial variation in RMS turbulence (u'/V_j) for a given z/d is plotted in Fig. 9 for two nozzle sizes at different Reynolds numbers. The data for $d = 10.9$ mm indicates a rise in turbulence level near $r/d = 1$, and both nozzle diameters exhibit increases in u'/V_j for $r/d \leqslant 2.5$. A distinct local maximum in the RMS turbulence is observed at $r/d \approx 2.5$. These trends suggest a transition to turbulent flow. Interestingly, the location of peak RMS turbulence seen in Fig. 9 corresponds to the point where the maximum radial velocity reaches the free surface (see Fig. 3). The radial location of this apparent transition point also coincides loosely to the local maximum in heat transfer coefficient observed previously for impinging free-surface liquid jets [17]. While the data are too sparse to draw definite conclusions, the location of transition does not appear to be strongly Reynolds number-dependent. Further, higher local turbulence levels are associated with higher Reynolds numbers.

Figure 10 illustrates local radial component turbulence intensity (u'/u) data inside the liquid layer for $d = 10.9$ mm, $Re = 53\,100$ at $z/d = 0.018$ and 0.046, as well as free-surface turbulence intensity (U'/U) data from ref. [13]. Values of the free-surface turbulence intensity extrapolated from the u'/u data of this study on the interior of the layer at the $z/d = 0.018$ and 0.046 locations are also included. The turbulence intensity measurements from inside the layer show a sudden sharp change at $r/d \approx 1$ with a local maximum observed in the $z/d = 0.018$ data near $r/d \approx 3$. The $z/d = 0.046$ profile is increasing, but has not reached a local maximum. The data illustrate that the free-surface turbulence intensity is a minimum at the radial location where, it has been suggested, transition to turbulence occurs and the peak mean velocity reaches the free surface. The free-surface turbulence level is seen to rise with radial position thereafter. Increased turbulence levels result near the wall at $r/d \approx 1$–2, and progress radially outward and upward inside the liquid layer. The extrapolated values for the free surface, though for a different nozzle and flow rate, follow the general shape of the data from ref. [13] confirming the validity of those measurements.

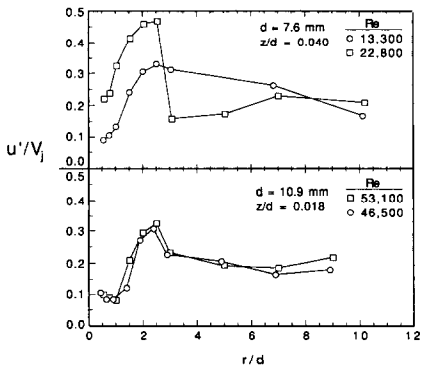

FIG. 9. Radial variation in RMS turbulence (u'/V_j) for a given z/d for two nozzle sizes at different Reynolds numbers.

CONCLUSIONS

The measurements from the interior of the radial-flow layer showed that the maximum velocity in the layer is not at the free surface for $r/d < 2.5$. This invalidates the assumptions of many analytical models for that portion of the flow. It also provides a physical explanation for the peak in free-surface velocities reported previously [13]. Various layer velocity profile assumptions were compared to available data taken at $r/d \approx 2$ and $r/d > 2$. Qualitatively, the profile assumptions were generally similar to the measured data, but there were insufficient data for thorough comparisons, particularly at $r/d > 2.5$ where agreement would be expected. Liquid layer depths

were calculated by integrating the measured layer velocity profiles and compared to various analytical predictions. The free-surface layer depth correlation of Stevens and Webb [13] and the turbulent model of Watson [1] accurately predicted an increase in depth of the liquid layer at larger r/d. Free-surface velocities were extrapolated from the measured data and compared to results reported in ref. [13] and agreement was very good. Turbulence was found to be highest near the impingement surface, and to increase gradually with r/d. An apparent transition to turbulence was observed in the radial flow layer, with a local minimum in the turbulence intensity (u'/u) near $r/d \approx 1$, and a peak in the RMS turbulence (u'/V_j) occurring near $r/d \approx 2.5$. This correlates well with the location of observed maxima in the local heat transfer coefficient from prior work [17].

Acknowledgements—This work was supported by the U.S. National Science Foundation under Grant No. CBT-8552493.

REFERENCES

1. E. J. Watson, The radial spread of a liquid jet over a horizontal plane, *J. Fluid Mech.* **20,** 481–499 (1964).
2. V. E. Nakoryakov, B. G. Pokusaev and E. N. Troyan, Impingement of an axisymmetric liquid jet on a barrier, *Int. J. Heat Mass Transfer* **21,** 1175–1184 (1978).
3. S. Thomas, A. Faghri and W. L. Hankey, The flow of a thin liquid film on a stationary and rotating disk—Part I: Experimental analysis and flow visualization. In *Heat Transfer in Space Systems* (Edited by S. H. Chan, E. E. Anderson, R. J. Simoneau, C. K. Chan, D. W. Pepper and B. F. Blackwell), HTD-Vol. 135, 125–133 (1990).
4. S. Thomas, W. Hankey, A. Faghri and T. Swanson, One-dimensional analysis of the hydrodynamic and thermal characteristics of thin film flows including the hydraulic jump and rotation, *ASME J. Heat Transfer* **112,** 728–735 (1990).
5. M. M. Rahman, A. Faghri and W. L. Hankey, Computation of turbulent flow in a thin liquid layer of fluid involving a hydraulic jump. In *Heat Transfer in Turbulent Flow* (Edited by R. S. Amano, M. E. Crawford and N. K. Anand), HTD-Vol. 138, 71–80 (1990).
6. M. M. Rahman, A. Faghri and W. L. Hankey, The flow of a thin liquid film on a stationary and rotating disk—Part II: Theoretical prediction. In *Heat Transfer in Space Systems* (Edited by S. H. Chan, E. E. Anderson, R. J. Simoneau, C. K. Chan, D. W. Pepper and B. F. Blackwell), HTD-Vol. 135, 135–142 (1990).
7. M. M. Rahman, A. Faghri, W. L. Hankey and T. D. Swanson, Prediction of heat transfer to a thin liquid film in plane and radially spreading flows, *ASME J. Heat Transfer* **112,** 822–825 (1990).
8. X. Liu and J. H. Lienhard V, Liquid jet impingement heat transfer on a uniform flux surface. In *Proceedings of the 1989 National Heat Transfer Conference*, HTD-Vol. 106, 523–530 (1989).
9. H. J. Carper, Impingement cooling by liquid jet. In *Porous Media, Mixtures and Multiphase Heat Transfer* (Edited by K. Vafai *et al.*), ASME HTD-Vol. 117, 23–30 (1989).
10. Y. T. Hung, A numerical analysis of jet impingement cooling of a rotating disk, M.S. Thesis, Texas Tech University, Lubbock, TX (1982).
11. R. G. Olsson and E. T. Turkdogan, Radial spread of a liquid stream on a horizontal plate, *Nature* **211,** 813–816 (1966).
12. T. Azuma and T. Hoshino, LDV measurement in radial flow of thin liquid film. In *Proceedings of the Osaka Symposium on Flow Measuring Techniques: The Application of LDV*, Association for the Study of Flow Measurements, Osaka, Japan, 1–15 (1983).
13. J. Stevens and B. W. Webb, Measurements of the free-surface flow structure under an impinging free liquid jet, *ASME J. Heat Transfer* **114,** 79–84 (1992).
14. J. Stevens, Y. Pan and B. W. Webb, Effect of nozzle configuration on transport in the stagnation zone of axisymmetric impinging free liquid jets: Part 1. Turbulent flow structure, *ASME J. Heat Transfer* **114,** 874–879 (1992).
15. Y. Pan, J. Stevens and B. W. Webb, Effect of nozzle configuration on transport in the stagnation zone of axisymmetric impinging free liquid jets: Part 2. Local heat transfer, *ASME J. Heat Transfer* **114,** 880–886 (1992).
16. J. Stevens, Measurements of local fluid velocities in an axisymmetric, free liquid jet impinging on a flat plate, Ph.D. Dissertation, Brigham Young University, Provo, UT (1991).
17. J. Stevens and B. W. Webb, Local heat transfer coefficients under an axisymmetric, single-phase liquid jet, *ASME J. Heat Transfer* **113,** 71–78 (1991).